Numerical Computation of the Nonlinear Far Field of Ultrasonic Waves Scattered by Closed Cracks of Various Orientations

Philippe Blanloeuil, Anissa Meziane, Andrew N. Norris, Mathieu Renier, Martin Veidt

7th European Workshop on Structural Health Monitoring
July 8-11, 2014. La Cité, Nantes, France

NUMERICAL COMPUTATION OF THE NONLINEAR FAR FIELD OF ULTRASONIC WAVES SCATTERED BY CLOSED CRACKS OF VARIOUS ORIENTATIONS

P. Blanloeuil[1], A. Meziane[2], A. N. Norris[3], M. Renier[2], M. Veidt[1]

[1] *School of Mechanical & Mining Engineering, University of Queensland, Brisbane, Australia*
[2] *Univ. Bordeaux, I2M, UMR 5295, F-33400 Talence, France.*
CNRS, I2M, UMR 5295, F-33400 Talence, France.
Arts et Metiers ParisTech, I2M, UMR 5295, F-33400 Talence, France.
[3] *Rutgers University, Mechanical and Aerospace Engineering, 98 Brett Road, Piscataway NJ 08854-8058, USA*

p.blanloeuil@uq.edu.au

ABSTRACT

The directivity patterns of the higher harmonics generated by the interaction between a bulk wave and a closed crack are obtained in the far field. A Finite Element (FE) model gives the near field solution which is then analytically propagated with expressions based on Hankel functions. The crack is modeled by an interface of unilateral contact with Coulomb's friction which takes into account a compression pre-stress σ_0 that closes the crack. The mode conversion occurring at the crack investigated. Moreover, the diffracted fields of the generated higher harmonics are compared to those of the fundamental harmonic.

KEYWORDS : *Nonlinear acoustics, Scattering, Higher Harmonics, Finite Elements.*

INTRODUCTION

The evaluation of damage at an early stage of fracture is relevant in many technologies. Ultrasonic methods based on linear wave scattering are efficient for detecting defects and characterizing material elasticity, but are less sensitive to micro-cracks or closed cracks. However, if the excitation amplitude is sufficient, the latter can behave nonlinearly because of contact dynamics occuring between the faces of the crack. This effect, called Contact Acoustic Nonlinearity (CAN) [1], has potential for characterization of closed cracks and is of great interest for the application of Structural Health Monitoring (SHM) using nonlinear ultrasonics.

Like classical nonlinearities [2], CAN generates higher harmonics [3]. This spectral enrichment has been largely studied on contacting interfaces [4, 5] and it has been shown that the nonlinear response is dependent on the normal stress applied on the interface. Higher harmonics generation has also been applied to closed cracks [6], which demonstrated its potential to reveal this kind of defect.

To set up a SHM method based on nonlinear acoustics, a good understanding of the nonlinear effects is necessary [7] as well as the propagation of the higher harmonics in the surrounding media. Moreover, if the crack is tilted (*e.g.* oblique incidence), mode conversions will occur, and each wave may carry the nonlinear signature of the crack. Therefore, it is interesting to obtain the directivity patterns corresponding to the higher harmonics and different wave modes in order to know in which directions these nonlinear components are preferentially generated.

The purpose of this paper is to examine the frequency content of waves scattered from a closed crack of different orientations. A two step procedure is used to plot the directivity pattern of the scattered field. First, a Finite Element (FE) model is used to solve the nonlinear problem of a wave interacting with a closed crack. The crack is pre-stressed and modeled by a unilateral contact with Coulomb's friction. Limited by the number of unknowns, the near field solution given by the FE model

is extended in the outside domain using an analytical method. This method uses Green's functions and is similar to the one used by Hunt et al. to compute the radiated field from elastic structures in a fluid domain [8]. The results provide valuable information about the higher harmonic propagation, especially regarding mode conversions.

1. FINITE ELEMENT MODEL

A Finite Element model using the software Plast2 [9] is built to treat the interaction between an acoustic wave and a crack of finite extent. An isotropic and homogeneous solid is considered, its mechanical properties are those of aluminum. The Young's modulus is $E = 69$ GPa, the Poisson's coefficient is $\nu = 0.33$ and the density is $\rho = 2700$ kg.m^{-3}. This solid contains a crack tilted by an angle θ. Perfectly matched layers (PML) are set on both sides of the solid to model an infinite solid in the direction $\boldsymbol{x}$. Finally, a plane wave of five cycles is generated on the top face of the solid. The central frequency of this pulse is 0.5 MHz for the shear wave and 1 MHz for the longitudinal wave. The wavelength of the incident waves is thus $\lambda \simeq 6$ mm. Finally, the amplitude of the incident wave is of 10 nm. Fig. 1 shows the characteristics of the model.

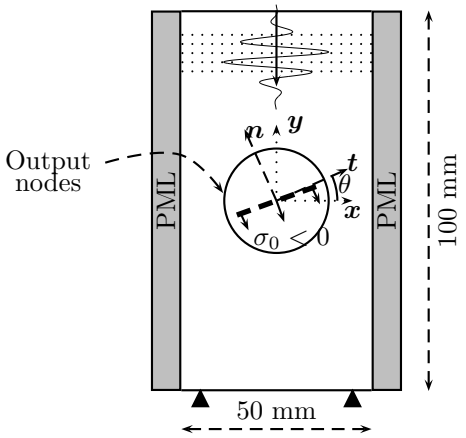

Figure 1 : Modeling of a wave interacting with a crack orientated by the angle θ. The length of the crack is $d = 10$ mm. The crack is represented by the dashed line and a pre-stress σ_0 is applied on the interface. The numerical output is defined on a circle of radius $R = 15$ mm.

The spatial discretization is essential in the FE method. In order to have an accurate solution up to the third harmonic, the corresponding wavelength has to be sufficiently discretized. The maximal size of the elements is $a = 0.2$ mm which means that the wavelength of the third harmonic is divided in ten elements ($\lambda_{3f}/a \simeq 10$). The mesh is refined at the vicinity of the crack tips because of the stress singularities ($\sigma \sim 1/\sqrt{r}$ where r is the radial distance from the crack tip). The software Plast2 uses a time explicit scheme and therefore the time step is subject to the Courant-Friedrichs-Lewy stability condition. The time step is $\Delta t = 3$ ns. The convergence has been validated in time and space. The displacements are recorded at each node belonging to a circle of radius $R = 15$ mm, as shown in Fig. 1. The length of the crack is $d = 10$ mm.

The crack is modeled by an interface of unilateral contact with Coulomb's friction. Therefore, three states can be observed simultaneously at different places of the interface: separation, slipping contact and sticking contact. The crack can be either closed by the weight of the structure or an external load or a residual stress due to plasticity. Therefore, it is assumed that a static normal stress $\sigma_0 < 0$ closes the crack. This pre-stress σ_0 is directly considered in the contact laws.

The crack is made of two faces which are denoted by $i = 1, 2$ respectively for the top and bottom face. Let be $\boldsymbol{u}^i$ the displacement and $\boldsymbol{n}^i$ the outward normal vector of the face i of the crack, the normal

jump of displacements is defined by:

$$[u_n] = \boldsymbol{u}^1 \cdot \boldsymbol{n}^1 + \boldsymbol{u}^2 \cdot \boldsymbol{n}^2 = (\boldsymbol{u}^1 - \boldsymbol{u}^2) \cdot \boldsymbol{n}^1 \tag{1}$$

The incident wave creates stresses represented by the Cauchy stress tensor $\boldsymbol{\sigma}(\boldsymbol{u}^i)$. Denoting $\sigma_n(\boldsymbol{u}^i)$ its normal component and $\tau(\boldsymbol{u}^i)$ its tangential component, the unilateral contact law taking into account σ_0 is given by the following equation:

$$\begin{cases} \sigma_n(\boldsymbol{u}^i) + \sigma_0 \leq 0 \\ [u_n] \leq 0 \\ (\sigma_n(\boldsymbol{u}^i) + \sigma_0).[u_n] = 0 \end{cases} \tag{2}$$

The first equation states that only a compression can be transmitted through the interface. The normal stress σ_n is allowed to be positive although the crack is closed as long as $\sigma_n \leq \mid \sigma_0 \mid$. When $\sigma_n = -\sigma_0$ the interface opens. The second line corresponds to the nonpenetration condition. Finally, the third line, or complementary condition, indicates that the contact interface is either open or closed.

Denoting μ the friction coefficient and $[u_t]$ the tangential jump of displacements, the Coulomb's law is used for the tangential behavior. The pre-stress σ_0 is also introduced in the classical law:

$$\begin{cases} \mid \tau(\boldsymbol{u}^i) \mid \leq \mu \mid \sigma_n(\boldsymbol{u}^i) + \sigma_0 \mid \\ \text{If } \mid \tau(\boldsymbol{u}^i) \mid < \mu \mid \sigma_n(\boldsymbol{u}^i) + \sigma_0 \mid \quad \Rightarrow \text{ sticking: } [u_t] = 0 \\ \text{If } \mid \tau(\boldsymbol{u}^i) \mid = \mu \mid \sigma_n(\boldsymbol{u}^i) + \sigma_0 \mid \quad \Rightarrow \begin{cases} \text{sliding: } \exists \alpha \geq 0; [u_t] = -\alpha \tau(\boldsymbol{u}^i) \\ \tau(\boldsymbol{u}^i) = \pm \mu \mid \sigma_n(\boldsymbol{u}^i) + \sigma_0 \mid \end{cases} \end{cases} \tag{3}$$

The shear stress τ has to be equal to $\mu \mid \sigma_n + \sigma_0 \mid$ to generate sliding. When sliding occurs, the value of the shear stress depends on the global normal stress $\sigma_n + \sigma_0$. The switches between the different contact states introduce the nonlinearity in the model. These boundary conditions can be referred as the non-smooth contact dynamics [10].

2. ANALYTICAL SOLUTION FOR THE RADIATED FIELD

The FE model gives the near field solution which is limited in space due to computational cost. The scattered field is defined as the difference between the total field and the incident field (obtained without the crack). Therefore, the crack is considered like a secondary source. The knowledge of the scattered field on the circle of radius $R = 15$ mm is used to obtain the solution in the far field, assuming that the material has a linear behavior. The cylindrical displacements obtained at $r = R$ are converted is the frequency domain using the Fourier transformation. Then, it is possible to obtain the radiated field for $r \geq R$ from an integral equation at $r = R$. This kind of approach has already been used in fluid mechanics [8].

The solution is assumed time harmonic, with the time convention $e^{-i\omega t}$. The displacements are written in the cylindrical coordinate system, in the frequency domain.

$$\hat{\boldsymbol{u}}(r,\theta) = \hat{u}_r \boldsymbol{e}_r + \hat{u}_\theta \boldsymbol{e}_\theta = \nabla\phi + \nabla \wedge \psi \boldsymbol{e}_z, \quad r \geq R, \tag{4}$$

where ϕ and ψ are respectively the velocity potential for the longitudinal wave and the shear wave. Then,

$$\hat{\boldsymbol{u}}(r,\theta) = \left(\frac{\partial \phi}{\partial r} + \frac{1}{r} \frac{\partial \psi}{\partial \theta} \right) \boldsymbol{e}_r + \left(\frac{1}{r} \frac{\partial \phi}{\partial \theta} - \frac{\partial \psi}{\partial r} \right) \boldsymbol{e}_\theta. \tag{5}$$

The velocity potentials have to satisfy the Helmholtz equation. Since we consider the waves scattered by a source located at the origin of the coordinate system, the potentials can be written with the Hankel's functions :

$$\begin{cases} \phi = \sum_n \frac{A_n}{k_L} H_n^{(1)}(k_L r) e^{in\theta} + \sum_n \frac{C_n}{k_L} H_n^{(2)}(k_L r) e^{in\theta} \\ \psi = \sum_n \frac{B_n}{k_T} H_n^{(1)}(k_T r) e^{in\theta} + \sum_n \frac{D_n}{k_T} H_n^{(2)}(k_T r) e^{in\theta} \end{cases} \tag{6}$$

where the notation $\sum_n = \sum_{n=-\infty}^{+\infty}$ is used. The terms $k_L = \omega/c_L$ and $k_T = \omega/c_T$ are respectively the wave numbers for the longitudinal wave and the shear wave. The scattered waves have to verify the Sommerfeld condition, which states that the radiated energy has to be zero at infinity. With the time dependence $e^{-i\omega t}$ and for a two dimensional space, this condition is given by:

$$\lim_{r\to\infty} \sqrt{r} \left(\frac{\partial}{\partial r} - ik \right) \hat{\boldsymbol{u}}(r,\theta) = 0. \tag{7}$$

The Sommerfeld condition is obtained when $C_n = 0, D_n = 0, \forall n$. Replacing the potential expressions in Eq. 5, the radial and the tangential displacements are given by:

$$\begin{cases} \hat{u}_r(r,\theta) = \sum_n A_n H_n^{(1)'}(k_L r) e^{in\theta} + \frac{in}{r} \sum_n \frac{B_n}{k_T} H_n^{(1)}(k_T r) e^{in\theta} \\ \hat{u}_\theta(r,\theta) = \frac{in}{r} \sum_n \frac{A_n}{k_L} H_n^{(1)}(k_L r) e^{in\theta} - \sum_n B_n H_n^{(1)'}(k_T r) e^{in\theta} \end{cases} \tag{8}$$

The coefficient A_n and B_n have now to be computed from an integral at $r = R$ where the displacements are known. To do that, each term of Eq. 8 is multiplied by $e^{-im\theta}$ and integrated over the circular domain. Using the orthogonality of the functions $e^{in\theta}$ for the scalar product $\langle f, g \rangle = \int_0^{2\pi} f(\theta) g(\theta) d\theta$, we obtain:

$$\begin{cases} \int_0^{2\pi} \hat{u}_r(R,\theta) e^{-im\theta} d\theta = 2\pi \left(A_m H_m^{(1)'}(k_L R) + \frac{in}{k_t R} B_m H_m^{(1)}(k_T R) \right) \\ \int_0^{2\pi} \hat{u}_\theta(R,\theta) e^{-im\theta} d\theta = 2\pi \left(\frac{im}{k_L R} A_m H_m^{(1)}(k_L R) - B_m H_m^{(1)'}(k_T R) \right) \end{cases}, \quad \forall m \tag{9}$$

Defining the matrix

$$\boldsymbol{M}_n(r) = \begin{pmatrix} H_n^{(1)'}(k_L r) & \frac{in}{k_T r} H_n^{(1)}(k_T r) \\ \frac{in}{k_L r} H_n^{(1)}(k_L r) & -H_n^{(1)'}(k_T r) \end{pmatrix}, \tag{10}$$

the coefficients A_n and B_n are the solution of a linear system, and are given by:

$$\begin{pmatrix} A_n \\ B_n \end{pmatrix} = \boldsymbol{M}_n^{-1}(R) \begin{pmatrix} \frac{1}{2\pi} \int_0^{2\pi} \hat{u}_r(R,\theta) e^{-in\theta} d\theta \\ \frac{1}{2\pi} \int_0^{2\pi} \hat{u}_\theta(R,\theta) e^{-in\theta} d\theta \end{pmatrix}. \tag{11}$$

Finally, the displacement field is obtained for any point of the outside domain from Eq. 8 and 11:

$$\hat{\boldsymbol{u}}(r,\theta) = \sum_n \boldsymbol{M}_n(r) \boldsymbol{M}_n^{-1}(R) \frac{e^{in\theta}}{2\pi} \int_0^{2\pi} \hat{\boldsymbol{u}}(R,\theta') e^{-in\theta'} d\theta' \quad , r \geq R, \forall \theta \tag{12}$$

This solution is valid for a given frequency. The directivity patterns are obtained by plotting the amplitude of the displacements over $\theta \in [0; 2\pi]$ for a radial distance $r = 100$ mm.

3. DIRECTIVITY PATTERNS

In this part, the directivity patterns are plotted for the fundamental frequency and the two first higher harmonics. Radial displacements u_r^* correspond to longitudinal waves and tangential displacements u_θ^* to shear waves. They are normalized by the maximal displacement measured at $r = R$ in the case of a linear simulation, *i.e* with free boundary conditions applied on the crack faces.

3.1 In-plane longitudinal wave

A longitudinal wave is considered and the directivity patterns are plotted in Fig. 2 for three orientations of the crack, $\theta = 0°, 25°, 45°$. The directions of propagation are marked by the dashed lines. Regarding the fundamental harmonic, the scattered displacement is mostly radial in the case of a normal incidence and the wave propagates in the same direction as the incident wave. There is no mode conversion. Under oblique incidence, the reflected wave propagates in the direction predicted by the Snell-Descartes law for simple reflection. Mode conversions occur and the reflected shear waves also propagate along the directions given by the Snell-Descartes law.

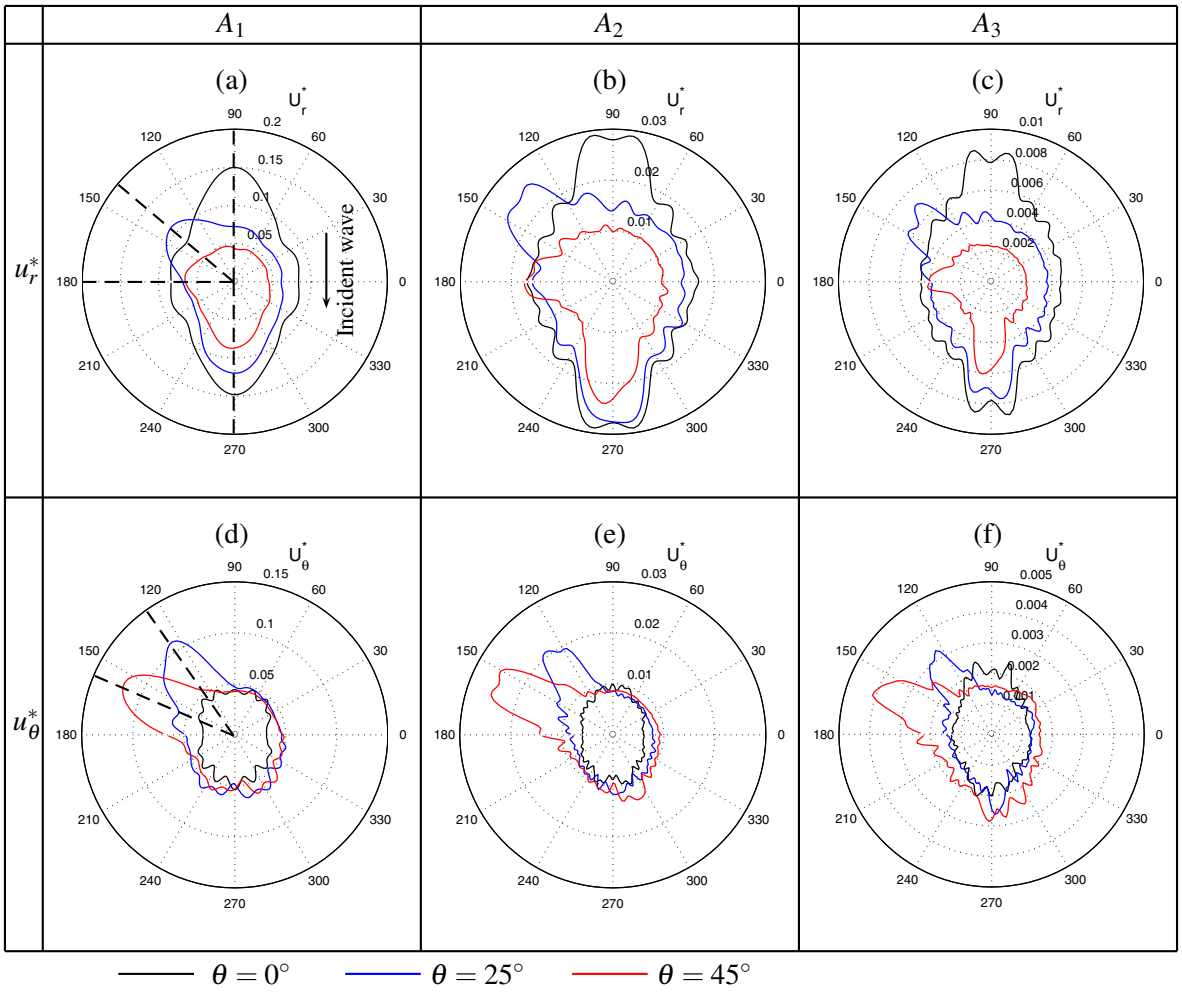

Figure 2 : Directivity patterns for an incident longitudinal wave, for $\theta = 0°, 25°, 45°$. (a), (b) and (c) give the radial displacements $\boldsymbol{u}_r^*$ for the fundamental and the two first higher harmonics. (d), (e) and (f) give the tangential displacements $\boldsymbol{u}_\theta^*$ for the same frequencies. $\sigma_0 = -0.15$ MPa and $\mu = 0.8$.

The second and the third harmonic are generated by the clapping occurring at the interface. These harmonics propagate in the same directions as the coresponding fundamental harmonic. However, the directivity seems enhanced in the case of the higher harmonics because of the shorter wavelength. As a consequence, the alignment of the transducers during a nonlinear experiment is a parameter that should be checked precisely, as demonstrated in [11]. The amplitude of the higher harmonics contained in the shear waves (Fig. 2.(e) and (f)) increases with the angle of incidence whereas it decreases for the longitudinal waves. The mode conversion is stronger for high incidence angle and more energy is transfered to the shear wave components.

3.2 In-plane shear wave

The directivity patterns are plotted in Fig. 3 for an incident shear wave. The directions of propagation are marked by the dashed lines. Three crack orientations are considered, $\theta = 0°, 25°, 45°$, and the directivity patterns are obtained for the fundamental and the two first higher harmonics. The contact parameters are $\sigma_0 = -0.25$ MPa and $\mu = 0.3$. In this case there is no activation of the clapping and only sliding is activated at the interface whatever the angle of incidence [7].

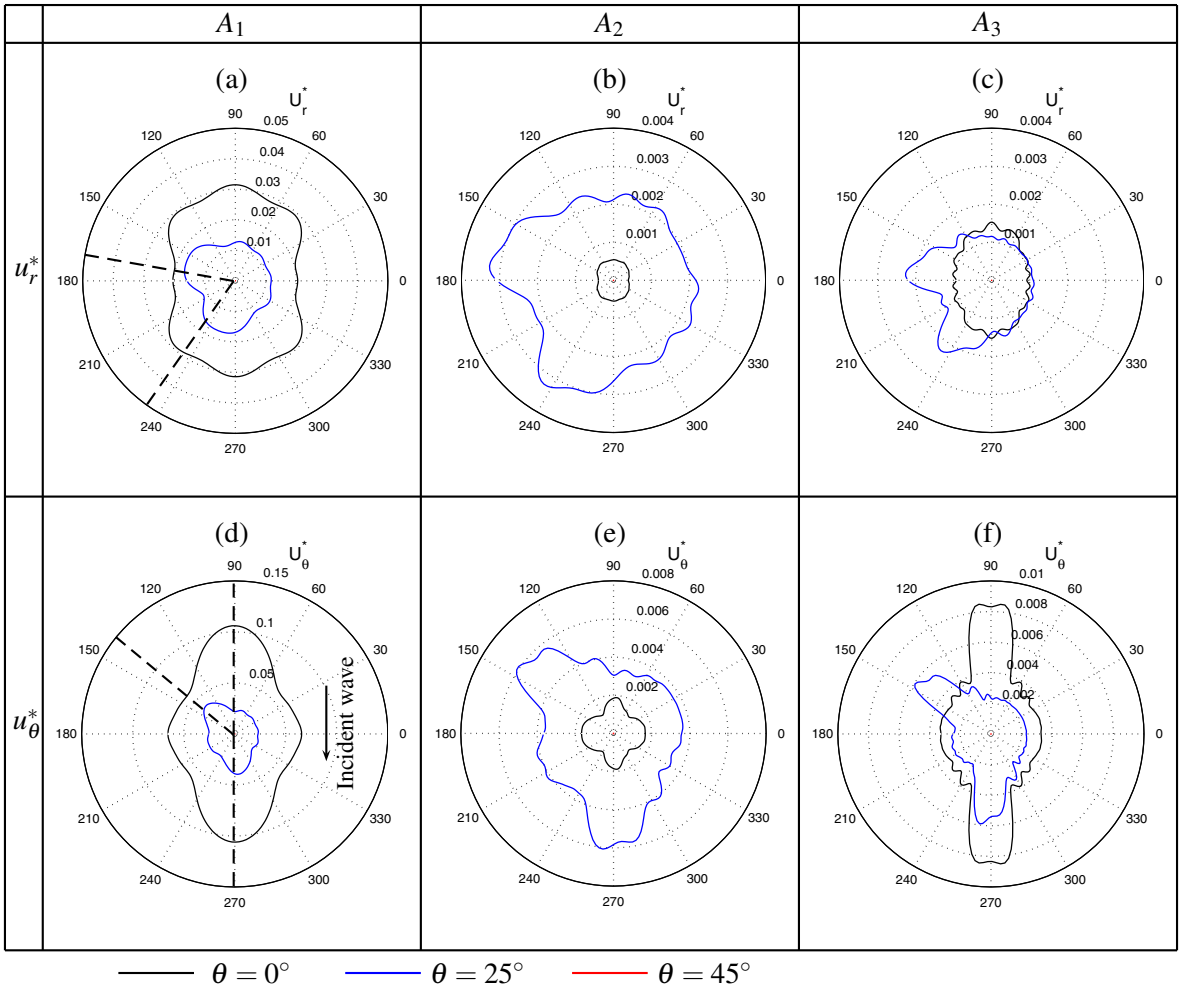

Figure 3 : Directivity patterns for an incident shear wave, for $\theta = 0°, 25°, 45°$. (a), (b) and (c) give the radial displacements $\boldsymbol{u}_r^*$ for the fundamental and the two fisrt higher harmonics. (d), (e) and (f) give the tangential displacements $\boldsymbol{u}_\theta^*$ for the same frequencies. $\sigma_0 = -0.25$ MPa and $\mu = 0.3$.

Similarly to the longitudinal wave, the higher harmonics, when they are generated, have directivity patterns of the same form as those of the fundamental harmonic. One can see that under normal incidence, the third harmonic is preferentially generated for the tangential displacements. Under oblique incidence, things get more intricate. For $\theta = 25^\circ$ mode conversions occur and there is an increase of the second harmonic, both for the tangential and the radial displacements. For $\theta = 45^\circ$ the values of the harmonics are insignificant and there are no scattered field. The reason can be understood under the consideration of contact stresses. An in-plane shear wave generates a shear stress $\sigma_{xy}(t)$ in the solid which maximal amplitude is 0.23 MPa. The normal and tangential stress generated by the incident wave at the interface are given by:

$$\begin{cases} \sigma_n^{inc}(t) = (\boldsymbol{\sigma}(t).\boldsymbol{n}).\boldsymbol{n} & = -\sigma_{xy}(t)\sin 2\theta \\ \tau^{inc}(t) = (\boldsymbol{\sigma}(t).\boldsymbol{n}).\boldsymbol{t} & = \sigma_{xy}(t)\cos 2\theta \end{cases} \tag{13}$$

where $\boldsymbol{\sigma}$ is the stress tensor and $\boldsymbol{n}$ and $\boldsymbol{t}$ are respectively the normal and tangent vector at the interface. For $\theta = 45$, the shear stress $\tau^{inc}(t)$ becomes zero and consequently it can not trigger sliding at the interface. The normal stress being to small to open the crack, there is no nonlinear effect and the wave propagation is not affected by the crack.

Directivity patterns of the scattered waves are closely linked to the orientation of the crack. It is well established that the nonlinear interaction between a wave and a closed crack is related to the state of stress at the interface. Other properties of the crack may also modify the scattering of higher harmonics. Here, the effect of the coefficient of friction μ is studied for a shear wave propagating with normal incidence. Since odd harmonics are mainly generated in this case, the directivity patterns of the third harmonics are plotted in Fig. 4.(a) for the tangential component and for different values of μ.

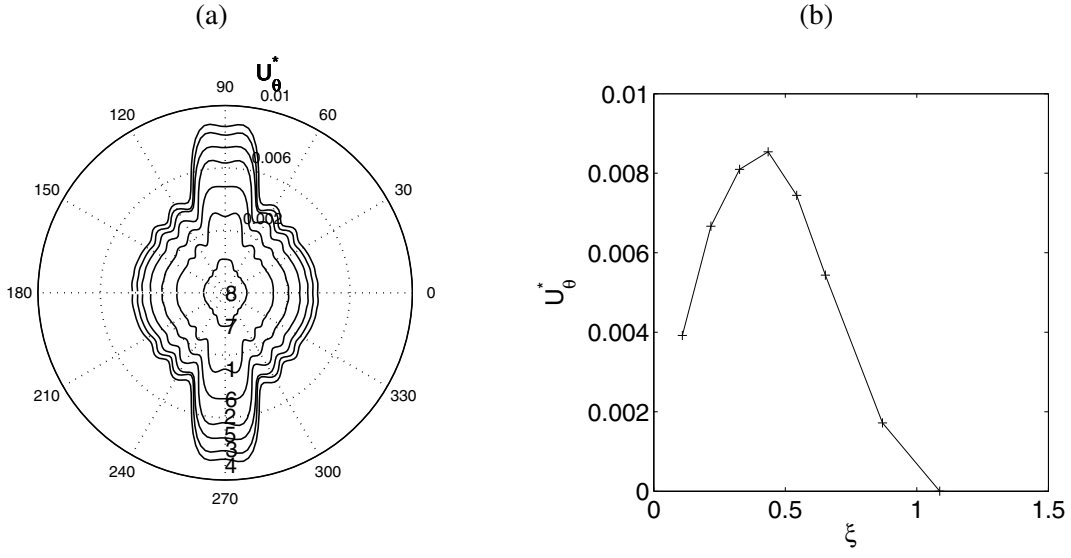

Figure 4 : The crack is horizontal. (a) The third harmonic directivity patterns of the tangential displacements $\boldsymbol{u}^*_\theta$ are plotted for different friction coefficients, respectively $\mu = 0.1, 0.2, 0.3, 0.4, 0.5, 0.6, 0.8, 1$ for the curves 1 to 8. The pre-stress is $\sigma_0 = -0.25$ MPa. (b) The amplitude of the third harmonic contained in the wave propagating in the direction 270° is plotted as a function of the normalized load ξ.

As expected, the third hamonic is mainly contained in the waves propagating along the direction normal to the interface. The coefficient of friction has only an amplitude effect on the third harmonic. Its amplitude is plotted in Fig. 4.(b) for the direction of propagation 270° as a function of the normal-

ized parameter ξ defined as :

$$\xi = \frac{\mu|\sigma_0 + \sigma_n^{inc}|}{|\tau^{inc}|} \tag{14}$$

The amplitude shows an optimal value which is obtained for $\xi \simeq 0.4$ ($\mu = 0.4$). This result agrees with previous work [12]. Under oblique incidence, the third harmonic still has an optimal value when the coefficient of friction changes but is obtained for a different value of ξ. This is due to mode conversion and energy transfer between the different waves.

CONCLUSION

In this paper, a Finite Element model is used to treat the nonlinear interaction between a plane wave and a closed crack, using an unilateral contact law with Coulomb's friction. The numerical solution computed at the near field is propagated semi-analytically to obtain the scattered field of the frequency components corresponding to the fundamental harmonic and the two first higher harmonics. The study of the directivity patterns provides valuable information about the higher harmonics propagation, especially regarding mode conversions. A major conclusion is that the direction of propagation of the higher harmonics agrees with those of the fundamental harmonic. The scattering behavior is also related to the mechanical properties of the crack, such as the state of stress or the coefficient of friction. This method enables computation of the scattered field at any position in the solid. It could be used to predict signals measured by transducers, and then help to position them to extract more information about closed cracks. A study of the influence of frequency should also be interesting for a SHM application.

REFERENCES

[1] I. Y. Solodov, N. Krohn, and G. Busse. CAN: an example of nonclassical acoustic nonlinearity in solids. *Ultrasonics*, 40:621–625, 2002.

[2] L. K. Zarembo and V. A. Krasil'nikov. Nonlinear phenomena in the propagation of elastic waves in solids. *Soviet Physics Uspekhi*, 13(6):778–797, 1971.

[3] O. Buck, W. L. Morris, and J. M. Richardson. Acoustic harmonic generation at unbonded interfaces and fatigue cracks. *Applied Physics Letters*, 33(5):371 –373, 1978.

[4] J. M. Richardson. Harmonic generation at an unbonded interface - I Planar interface between semi-infinite elastic media. *International Journal of Engineering Science*, 17(1):73 – 85, 1979.

[5] S. Biwa, S. Yamaji, and E. Mastumoto. Quantitative evaluation of harmonic generation at contacting interface. *American Institute of Physics*, 978(0), 2008.

[6] T. H. Lee and K. Y. Jhang. Experimental investigation of nonlinear acoustic effect at crack. *NDT & E International*, 42:757–764, 2009.

[7] P. Blanloeuil, A. Meziane, and C. Bacon. Numerical study of nonlinear interaction between a crack and elastic waves under an oblique incidence. *Wave Motion*, (0):–, 2013.

[8] J. T. Hunt, M. R. Knittel, and D. Barach. Finite element approach to acoustic radiation from elastic structures. *The Journal of the Acoustical Society of America*, 55(2):269–280, 1974.

[9] L. Baillet and T. Sassi. Mixed finite element methods for the Signorini problem with friction. *Numerical Methods for Partial Differential Equations*, 22(6):1489–1508, 2006.

[10] M. Jean. The non-smooth contact dynamics method. *Computer Methods in Applied Mechanics and Engineering*, 177(3–4):235 – 257, 1999.

[11] S. Liu, A. J. Croxford, S. A. Neild, and Z. Zhou. Effects of experimental variables on the nonlinear harmonic generation technique. *IEEE Transactions on Ultrasonics, Ferroelectrics and Frequency Control*, 58:1142–1451, 2011.

[12] A. Meziane, A. N. Norris, and A. L. Shuvalov. Nonlinear shear wave interaction at a frictional interface: Energy dissipation and generation of harmonics. *Journal of the Acoustical Society of America*, 130(4):1820–1828, 2011.